Desalination and Water Treatment
www.deswater.com
doi: 10.1080/19443994.2013.764488

51 (2013) 6082–6090
September

Taylor & Francis
Taylor & Francis Group

Synthesis and characterization of Pt–ZnO-hydroxyapatite nanoparticles for photocatalytic degradation of benzene under visible light

R.M. Mohamed[a,b,c,*], E. Aazam[a]

[a]*Chemistry Department, Faculty of Science, King Abdulaziz University, P.O. Box 80203, Jeddah, 21589, Saudi Arabia*
Tel. +966 540715648; Fax: +966 2 6952292; email: rmmohammed@kau.edu.sa
[b]*Advanced Materials Department, Central Metallurgical R&D Institute, CMRDI, P.O. Box 87 Helwan, Cairo, Egypt*
[c]*Center of Excellence in Environmental Studies, King Abdulaziz University, P.O. Box 80216, Jeddah, 21589, Saudi Arabia*

Received 3 December 2012; Accepted 5 January 2013

ABSTRACT

Hydroxyapatite modified Pt–ZnO nanoparticles (Pt–ZnO –HAP) were synthesized by a template-ultrasonic assisted method. The nanoparticles were characterized by X-ray diffraction, UV–Vis absorption spectroscopy, N_2 adsorption–desorption measurement (Brunauer, Emmett and Teller [BET]), photoluminescence spectroscopy, etc. The photocatalytic activities were evaluated by a photocatalytic oxidation decomposition of benzene under a visible-light irradiation. The results showed that the coupled system (Pt–ZnO –HAP) indicated a maximum photocatalytic activity and photochemical stability under a visible-light irradiation than all the other catalysts. The intensively improved visible-light-induced photocatalytic activity of the Pt–ZnO –HAP hybrids could be attributed to its strong absorption in the visible-light region, low recombination rate of the electron–hole pair, and large BET specific surface area.

Keywords: Hydroxyapatite modified Pt–ZnO; Visible light; Benzene removal

1. Introduction

Benzene is a typical pollutant that is commonly found in the atmosphere of both domestic and industrial areas. Especially in indoor environment, it would make a great influence on human health for its high toxicity and carcinogenicity [1]. Therefore, it is meaningful to develop an efficient technology to remove benzene from the ambient environment. To this day, a variety of gas–solid heterogeneous photocatalytic processes have been studied to remove the volatile organic compounds including benzene [2–5]. By using nano-semiconductor catalysts, these organic contaminants can be ultimately converted into water vapor (H_2O) and carbon dioxide (CO_2) at room conditions. Titanium dioxide (TiO_2) has been proved to be the most suitable option owing to its physical and chemical stability, strong oxidizing power, and the economical characteristics. In the process of TiO_2 gas–solid photocatalysis, the primary aspect resides on the adsorption of pollutants onto the active sites of TiO_2 surface. However, one main drawback of TiO_2 is the poor adsorption

*Corresponding author.

capacity towards some non-polar organic molecules due to its polar surface [6,7]. To overcome the problem, numerous researchers are focusing on mixing some adsorbents with TiO_2 to improve the adsorptive ability. It has been documented that the adsorption activity towards gas pollutants was efficiently enhanced for the hybridization of TiO_2 nanoparticles with adsorbents, such as activated carbon [8,9], zeolites [10,11], pillared clay [12,13], and silica [14]. Hydroxyapatite (HA) can be considered as a good applicant for supporting material due to its transparency and excellent adsorption properties toward different aqueous and air pollutants [15–18]. Thus, HA was utilized for water purification from heavy metals [16,17]. HA coated organic substrates showed high adsorption ability to damaging VOCs such as formaldehyde [18]. HA was also used as NO_2 collector [15]. Furthermore, it was reported that HA shows its own photocatalytic activity [19–23] in degradation of several toxic organic compounds in aqueous solution or in gaseous phase. Extremely good results on photocatalytic decay over HA were observed for methylene blue [22], methyl mercaptane [20,21], dimethyl sulfide [22], and azo dyes [23]. It was suggested that the photocatalytic activity of HA is caused by the generation of active superoxide anion radicals ($O_2\bullet-$) due to change in the electronic state of surface PO_4^{3-} group under UV irradiation [20–23]. There are also some announcements for HA/TiO_2 composites where the adsorption properties of HA are joint with the photocatalytic properties of TiO_2 [15,19,24,25]. Thus, the decay of methylene blue [19] and methylene orange [25] on HA/TiO_2 particles was much quicker than that on HA or TiO_2 powder alone. This result was assigned to the strong adsorption of the reaction intermediates on HA and to their subsequent transfer to TiO_2. The HA/TiO_2 film showed better decay effect on formaldehyde gas in comparison with that of the bare TiO_2 that was explained by synergetic effect of high photocatalytic activity of TiO_2 and high adsorption ability of HA [25].

In the study, in order to find a kind of material with enhanced adsorption and photocatalytic performance, hydroxyapatite modified Pt–ZnO nanoparticles (Pt–ZnO–HAP) were synthesized by a template-ultrasonic assisted method. The photocatalytic activities were evaluated by photocatalytic decay of benzene under a visible-light irradiation.

2. Experimental section

2.1. Preparation of HA

The preliminary materials used in the synthesis of nanohydroxyapatite (HAP) includes calcium nitrate tetra hydrate ($CaNO_3{\cdot}4H_2O$), diammonium hydrogen orthophosphate $(NH_4)_2HPO_4$, glycine (NH_2CH_2COOH), acrylic acid ($CH_2CHCOOH$), and sodium hydroxide (NaOH). All the chemicals used were of analytical grade and the aqueous solutions were made by dissolving them in double distilled water. The experimental procedure used to synthesize the HAP nanoparticles is shown in Fig. 1.

To prepare a transparent precursor for calcium, 1.2 g of calcium nitrate (0.05 mol/L) was dissolved in 100 mL of double distilled water. At the same time, 0.4 g of diammonium hydrogen orthophosphate (0.03 mol/L) was also dissolved in 100 mL of double distilled water for phosphate precursor. The aqueous solutions of calcium nitrate tetrahydrate and diammonium hydrogen orthophosphate were first mixed slowly with constant stirring, and then the mixture was placed in a magnetic stirrer for about 6 h. The ratio of Ca: P in the mixture was maintained at 1.6. To the above mixture, 0.1 M glycine and 0.1 M acrylic acid were also added and carefully mixed using a magnetic stirrer for about 24 h at room temperature,

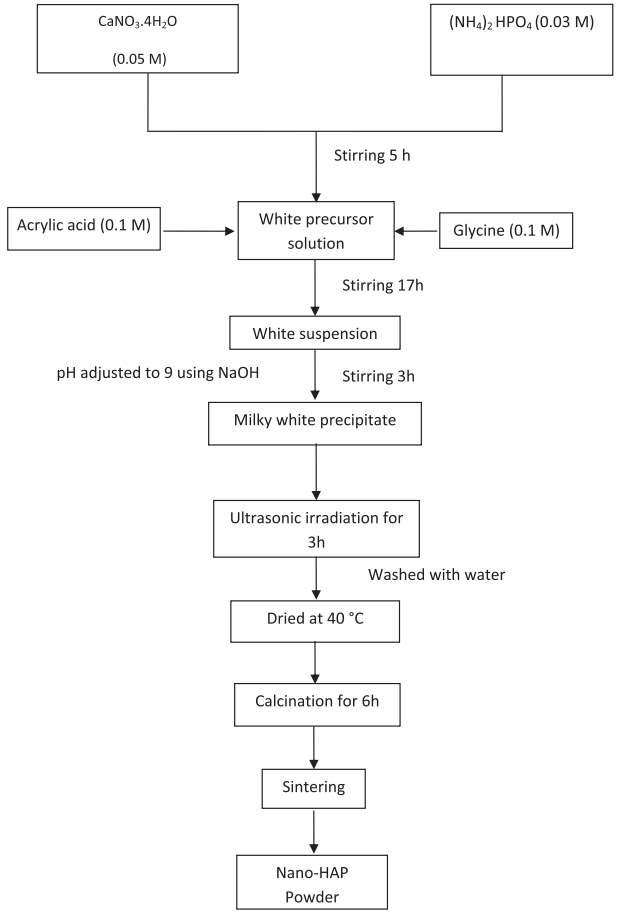

Fig. 1. Flow chart for the synthesis of nanohydroxyapatite particles.

and the pH of the mixture was adjusted to nine using sodium hydroxide. A milky white precipitate thus obtained was strongly stirred for another 6 h and then pushed into ultrasonicator at the frequency of 28 kHz and the power used is 150 W for 2 h irradiation time. The resulting precipitate was filtered and washed with double distilled water to remove nitrate ion and the organic moieties enclosed in the as-synthesized powder then dried at about 40˚C for 24 h. The dried powder was further calcined for about 5 h and followed by sintering in a muffle furnace for 3 h.

2.2. Preparation of ZnO

Diethyl zinc was selected as a precursor of Zn. Firstly, 3 mL diethanolamide was dissolved in 10 mL ethanol. Afterwards, diethyl zinc was added dropwise into the above solution under strong stirring for 2 h at room temperature. Finally, the gel was dried at 110˚C for 24 h, heat treated at 550˚C for 5 h, and then ground to obtain ZnO nanoparticles.

2.3. Preparation of Pt–ZnO

Firstly, 3 mL diethanolamide was dissolved in 10 mL ethanol. Afterwards, diethyl zinc was added dropwise into the above solution under strong stirring; then, a definite amount of platinum (II) chloride ($PtCl_2$) dissolved by ethanol was added into the mixture. The weight percentage of Pt to ZnO was controlled to be 5%. During the synthesis, the mixtures were stirred at 400–500 rmp for 2 h at room temperature. Finally, the gel was dried at 110˚C for 24 h, heat treated at 550˚C for 5 h, and then ground to obtain Pt–ZnO nanoparticles.

2.4. Preparation of Pt–ZnO –HAP

3 mL diethanolamide was dissolved in 10 mL ethanol. Afterwards, diethyl zinc was added dropwise into the above solution under strong stirring; then, a definite amount of platinum (II) chloride ($PtCl_2$) dissolved by ethanol, was added into the mixture. The weight percentage of Pt to ZnO was controlled to be 5 wt.%. During the synthesis, the mixtures were stirred at 400–500 rmp for 2 h at room temperature. Whereafter, the calculated amount of HA was dispersed in 5 mL n-hexane and was added into the solution such that the weight percentage of ZnO to HAP is 75 wt.%. The mixed solution was continuously stirred. Finally, the gel was dried at 110˚C for 24 h, heat treated at 550˚C for 5 h, and then ground to obtain the Pt–ZnO –HAP nanoparticles.

2.5. Characterization techniques

X-ray diffraction (XRD) analysis was carried out at room temperature using a Bruker axis D8 by Cu Kα radiation ($\lambda = 1.540$ Å). Specific surface area was calculated from measurements of N_2-adsorption using a Nova 2000 series Chromatech apparatus at 77 K. Prior to the measurements, all samples were treated under vacuum at 250˚C for 2 h. Band-gap of the samples was identified by UV–Visible diffuse reflectance spectra (UV-Vis-DRS) in air at room temperature in the wavelength range of 200–800 nm using a UV/Vis/NIR spectrophotometer (V-570, JASCO, Japan). Transmission electron microscopy (TEM) was recorded with a JEOL-JEM-1230 microscope, the prepared samples were prepared by suspending the prepared samples in ethanol, followed by ultrasonication for 30 min; then, a small amount of this solution was added onto a carbon-coated copper grid and dryied before loading the sample in the TEM. The X-ray absorption fine structure (XAFS) analysis, X-ray absorption near edge structure, and extended X-ray absorption fine structure (EXAFS) were performed at BL-7C facility of the Photon Factory at the National Laboratory for High-Energy Physics, Tsukuba, Tokyo, Japan. The K-edge XAFS spectra of Pt was measured in the fluorescence mode at 298 K and Fourier transformed was performed on k^3-weighted EXAFS oscillations in the range of 1–10 $Å^{-1}$.

2.6. Analysis of hydroxyl radicals ($^{\bullet}OH$)

The analysis of $^{\bullet}OH$ radical's formation on the sample surface was measured by the photoluminescence (PL) technique using terephthalic acid as a probe molecule, which readily reacted with $^{\bullet}OH$ radicals to produce a highly fluorescent product The method relies on the PL signal at 425 nm of 2-hydroxyterephthalic acid, the PL intensity of 2-hydroxy terephthalic acid is proportional to the amount of $^{\bullet}OH$ produced on the surface of ZnO [26].

Experimental procedures were as follows: at ambient temperature, 0.1 g of catalyst sample was dispersed in 20 mL of the 5×10^{-4} M terephthalic acid aqueous solution with a concentration of 2×10^{-3} M NaOH in a dish with a diameter of about 9.0 cm. A 125-W high-pressure Hg lamp (10 cm above the dishes) was used as a light source. PL spectra of the generated 2-hydroxyterephthalic acid were measured on a fluorescence spectrophotometer Shimadzu RF-530. After irradiation, every 10 min, the reaction solution was filtrated to measure the increase in the PL intensity at 425 nm.

2.7. Photocatalytic degradation experiment

The photocatalytic experiments were carried out in a closed cylindrical reactor made of stainless steel,

and the roof was equipped with a 150-W high-pressure mercury lamp doubly covered with a UV cut filter. The intensity data of UV light is confirmed to be under the detection limit (0.1 mW/cm^2) of a UV radiometer. The aqueous suspension of catalyst powders (0.5 g) was coated on a glass dish with a diameter of 16.0 cm, and then dried at 70°C. After the glass dish was set inside the reactor, 10 μL of liquid benzene was injected, and the lamp was turned on. A gas chromatograph (Agilent GC 7890A model) was connected to the reactor, and further used to analyze the gas composition in the reactor. The photocatalytic efficiency was defined as the measured amount of produced carbon dioxide divided by the expected amount of carbon dioxide produced from the injected benzene [27]. Procedures for the recycled experiments are as follows: when the first photocatalytic experiment ended, the reactor was opened to remove the photocatalytic products (mainly CO_2), and then was covered again. After that, 10 μL of benzene was injected in the reactor for another time, the lamp was turned on, and the next cycle of photocatalytic oxidation of benzene started. These cycles were repeated for 10 times. The adsorption capacity of the catalysts was measured similar to that of photocatalytic activity measurements. The only difference is that the adsorption process was carried out without light irradiation.

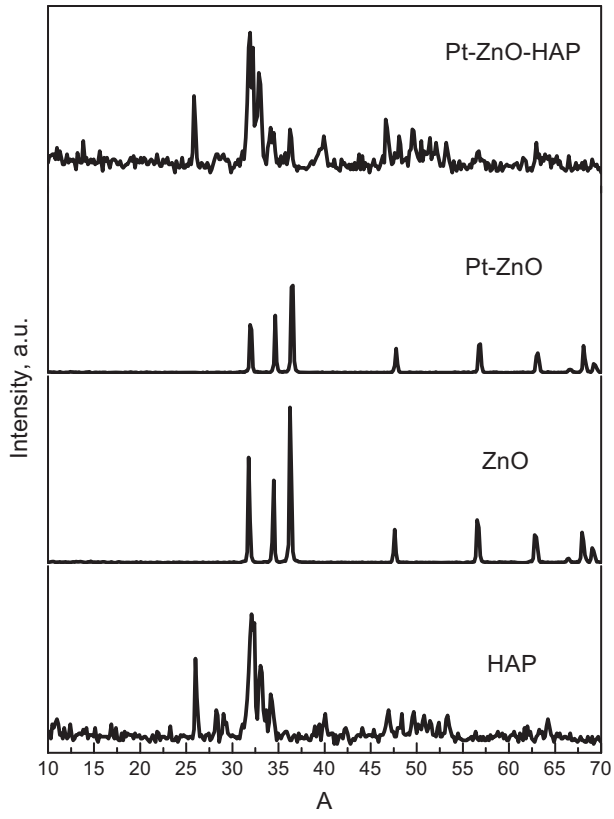

Fig. 2. XRD patterns of HAP, ZnO, Pt–ZnO, and Pt–ZnO –HAP.

3. Results and discussion

3.1. XRD and EXAFS analysis

XRD is used to investigate the phase structure and the phase composition of materials. Fig. 2 shows that the XRD patterns of HAP, ZnO, Pt–ZnO, and Pt–ZnO–HAP, respectively. The crystallinity of the HAP is confirmed by the reflections observed at 2θ values of 25.8°, 31.7°, 32.17°, 33.0°, 39.8°, 46.6°, and 49.5° (JCPDS cards No.74-565). The ZnO (JCPDS cards No.89-0510) could be observed in pure ZnO and its corresponding hybrids (Pt–ZnO, Pt–ZnO–HAP). Also, the HAP (2θ values of 25.8°, 31.7°, 32.17°, 33.0°, 39.8°, 46.6°, and 49.5° (JCPDS cards No.74-565) could be observed in Pt–ZnO –HAP.

To investigate the nature of the Pt introduced into the hybrids, we performed EXAFS measurements. Fig. 3 shows the EXAFS analysis for Pt–ZnO–HAP and Pt–ZnO. The presence of the peaks assigned to the Pt–Pt at about 2.50 Å indicates the formation of nano-sized Pt. The intensity of the Pt-Pt peak of the Pt–ZnO–HAP catalyst is lesser than that of the Pt–ZnO catalyst.

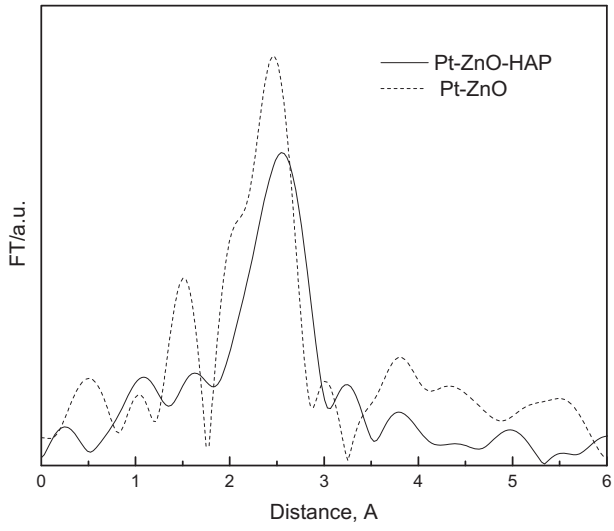

Fig. 3. Fourier transforms of Pt LIII-edge EXAFS spectra for Pt–ZnO and Pt–ZnO–HAP.

3.2. UV–Vis diffuse reflectance spectra

The light absorption characteristics of different samples were measured with UV–Vis diffuse

spectroscopy (Fig. 4). From the results, it can be seen that the HAP shows no apparent absorption in the range of 250–800 nm. The undoped ZnO and P_{25} show spectra with absorption sharp edge rising at 402 nm. An apparent absorption peak around 471 nm in the visible range was observed for the Pt–ZnO nanoparticles; it is the characteristic of surface plasma absorption corresponding to Pt particles [28]. The absorption spectrum of Pt–ZnO–HAP is like that of Pt–ZnO, which infers that both Pt–ZnO and Pt–ZnO–HAP can effectively enlarge light absorption to the range of visible light. Therefore, the doping of Pt to ZnO reduces the band gap of ZnO about 17%; besides, the doping of both (Pt and HAP) to ZnO reduces to about 24%.

3.3. BET

Fig. 5 shows the nitrogen adsorption–desorption isotherms and Brunauer, Emmett and Teller (BET) surface area of different catalysts. All the samples show the isotherms of type IV, with a hysteresis loop at relative pressure (P/P^0) between 0.4 and 1.0, indicating the presence of mesopores. As shown in Fig. 5, the order of BET specific surface areas is as follows: Pt–ZnO–HAP > Pt–ZnO > P_{25} > ZnO. It is widely accepted that photocatalysts with high specific surface areas and porous structures are favorable to the enhancement of photocatalytic performance. So, Pt–ZnO–HAP hybrids are expected to exhibit improved photocatalytic performance. Therefore, the doping of Pt to ZnO enhances the surface area of ZnO about 200%; whereas the doping of both (Pt and HAP) to ZnO enhances the surface area of ZnO about 400%.

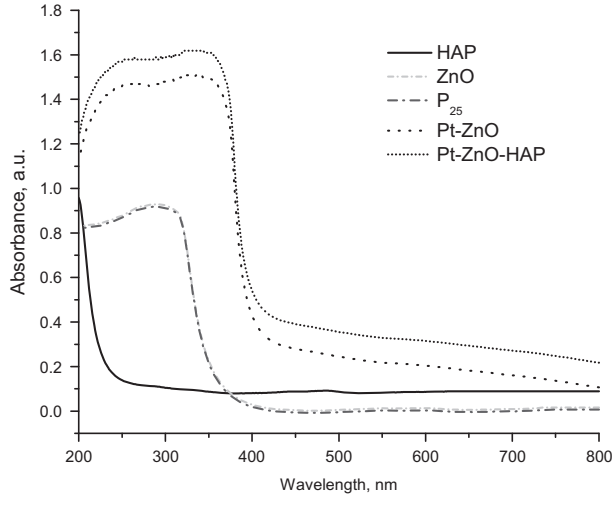

Fig. 4. UV-Vis absorption of HAP, ZnO, Pt–ZnO, and Pt–ZnO –HAP.

3.4. PL spectra

PL emission spectra can be used to investigate the outcome of photogenerated electrons and holes in a semiconductor, since PL emission results from the recombination of free charge carriers. Fig. 6(A) shows the change of PL spectra with irradiation time for Pt–ZnO–HAP samples in terephthalic acid solution. A gradual increase in PL intensity at about 425 nm is observed with increasing irradiation time; however, no PL increase is observed in the absence of visible light or Pt–ZnO–HAP samples. This suggests that the fluorescence is from the chemical reactions between terephthalic acid and $^{\bullet}OH$ formed at the Pt–ZnO–HAP/water interface via photocatalytic reactions.

Fig. 6(B) shows the change of PL spectra with irradiation time for different samples. Usually, PL intensity is proportional to the amount of hydroxyl radicals produced. It can be easily seen that at a fixed time (60 min), the formation rate of OH radicals on the Pt–ZnO nanoparticles is much faster than that of the undoped ZnO and P_{25}; this implies that the Pt–ZnO nanoparticles have higher visible-light photocatalytic activity than undoped ZnO and P_{25}. Especially, the Pt–ZnO–HAP sample has the strongest PL intensity, implying the highest photocatalytic activity. The reason may be that the Pt adsorbed on the surfaces of ZnO can attract the photogenerated electrons and then reduce the recombination rate of the photogenerated electrons and holes. Therefore, large amounts of separated electrons and holes exist on the surface of the Pt–ZnO and Pt–ZnO–HAP samples; the excessive electrons and holes are accepted by surface adsorbed O_2 and H_2O, and this formed more $^{\bullet}OH$ radicals to participate in the photocatalytic reaction. What is more, the OH radicals generated on the surface of Pt–ZnO –HAP samples are more inclined to remain adsorbed on their surface for their much stronger adsorption ability than the other samples.

3.5. TEM

The TEM images of samples are shown in Fig. 7. As can be seen from the images, HAP shows rod-like structures in the range of about 50–100 nm length and 10–25 nm width. For the Pt–ZnO–HAP samples, the Pt–ZnO nanocrystals with diameter of about 9 nm can be clearly seen on the surface of HAP nanorod.

3.6. Adsorption and photocatalytic activity

The dark adsorption study of benzene on supported catalysts is presented in Table 1. After 1 h in the dark, about 22% benzene was adsorbed by HAP,

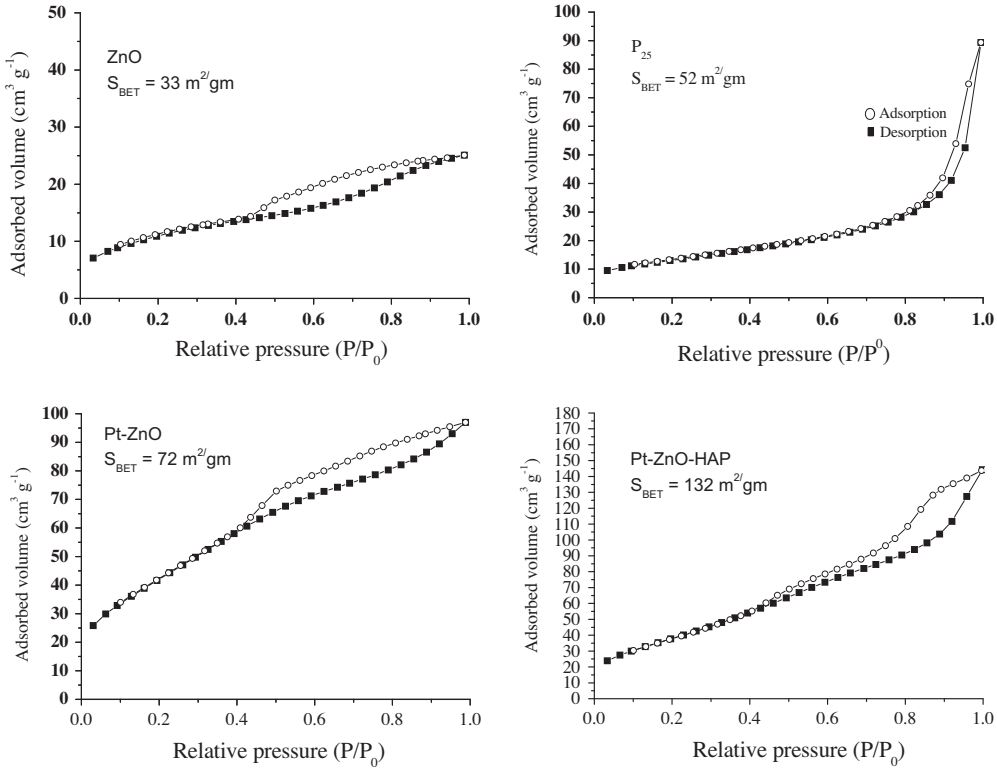

Fig. 5. N_2 adsorption–desorption isotherms.

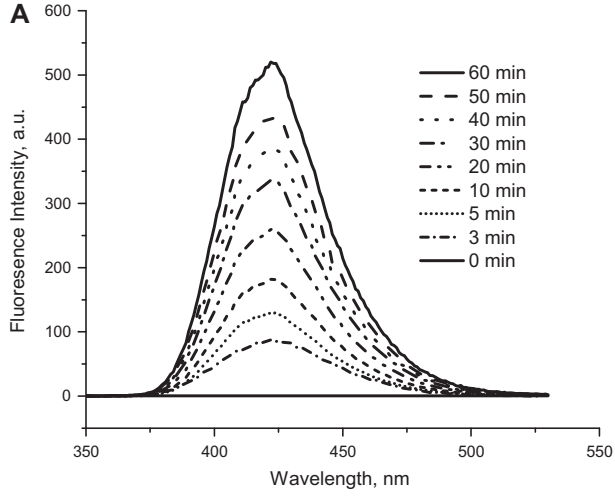

Fig. 6(A). Fluorescence spectral changes in 5×10^{-4} M NaOH solution of terephthalic acid for Pt–ZnO–HAP.

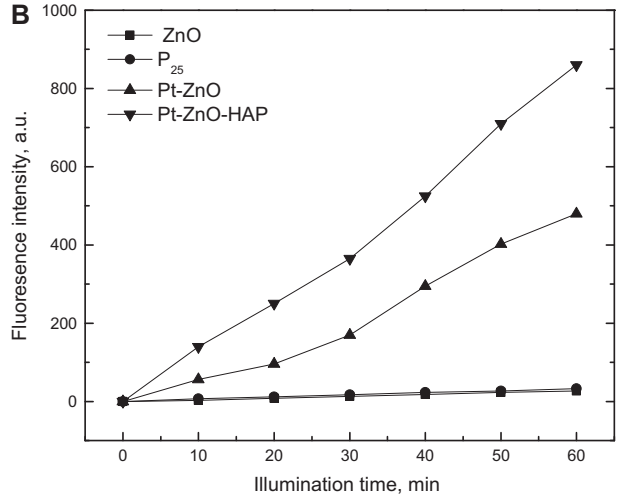

Fig. 6(B). Fluorescence spectral changes in 5×10^{-4} M NaOH solution of terephthalic acid for different catalysts.

5% benzene was adsorbed by Pt–ZnO–HAP, and 3% benzene was adsorbed by Pt–ZnO; but adsorption of benzene by the undoped ZnO and P_{25} in the same time is approximately zero (Table 1). After 2 h in the dark, the adsorption of benzene almost remained unchanged; this means that adsorption equilibrium can be reached after 1 h in the dark.

The kinetics of photocatalytic degradation of benzene and the apparent reaction rate constant k of different samples are shown in Fig. 8. The undoped ZnO and P_{25} samples show poor photocatalytic activities in visible-light region, which can be assigned to the large band gap. The photocatalytic activity of Pt–ZnO sample is much higher than that of the pure ZnO and P_{25}

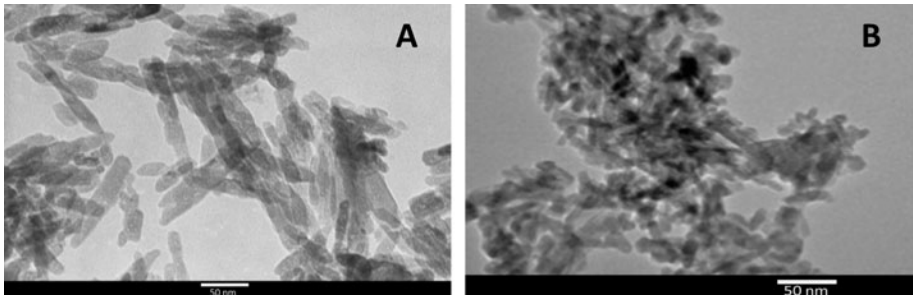

Fig. 7. TEM images of HAP (A) and Pt–ZnO– HAP (B).

Table 1
Adsorptive ability of the catalysts for benzene

Sample	Adsorption % of Benzene after 1 h	Adsorption % of Benzene after 2 h
HAP	20	22
ZnO	0	0
P_{25}	0	0
Pt–ZnO	3	4
Pt–ZnO– HAP	5	6

and its rate constant k reaches 0.009 min^{-1}. The Pt-ZnO–HAP composite shows the highest photocatalytic activity and its k value is 0.026 min^{-1}, which is 2.88 times that of Pt–ZnO and 13 times that of P_{25}, respectively.

In a typical photocatalytic reaction, photogenerating electrons and holes are captured by O_2 and H_2O absorbed by ZnO forming superactive $^{\bullet}OH$, $^{\bullet}O_2^-$, and $^{\bullet}OOH$ oxidants which decompose benzene on the surface of ZnO. Therefore, the effective separation of electron–hole pairs, or the enhanced photodegradation of benzene can be promoted by the increase in the concentration of surface hydroxyl groups and adsorbed molecular oxygen. In this study, after modified by Pt and HAP, the S_{BET} and the content of hydroxyl groups increase significantly. On the one hand, the catalysts with higher specific surface areas can provide greater reaction platform for organic pollutants decomposition. On the other hand, the increase of amount of hydroxyl not only increases the trapping sites for photogenerated holes, but also can increase the trapping sites for photogenerated electrons by adsorbing more molecular oxygen, resulting in more hydroxyl radicals to participate in the photocatalytic reaction. As a result, Pt–ZnO–HAP shows the highest photocatalytic activity than all the other catalysts. Fig. 9 shows the mechanism of photocatalytic oxidation of benzene by Pt–ZnO–HAP

3.7. Photochemical stability

To evaluate the photochemical stability of the catalyst, the repeated experiments for the

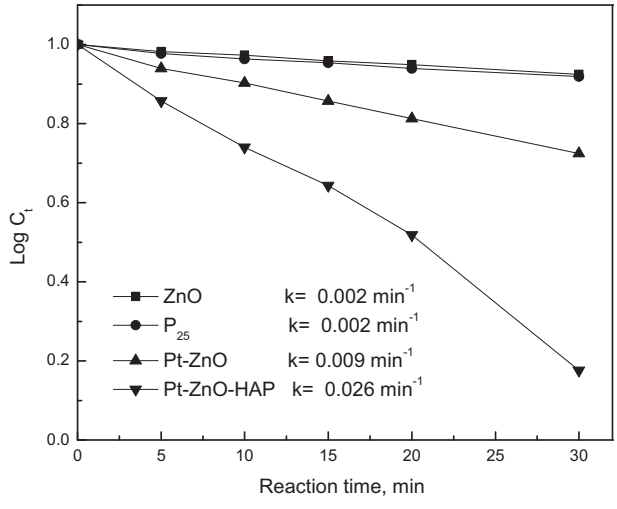

Fig. 8. Photocatalytic degradation of benzene by ZnO, P_{25}, Pt–ZnO, and Pt–ZnO –HAP.

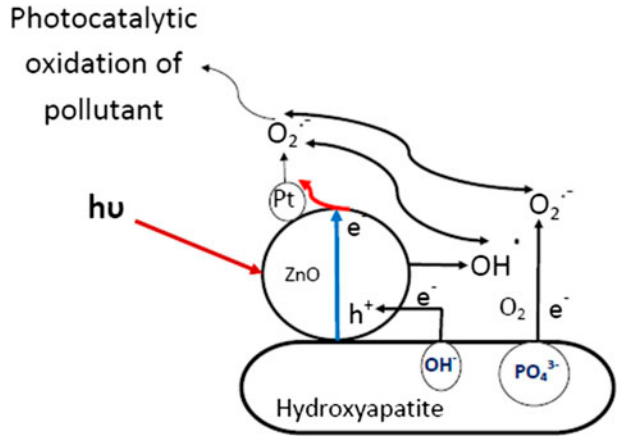

Fig. 9. Photocatalytic mechanism of benzene by Pt–ZnO –HAP.

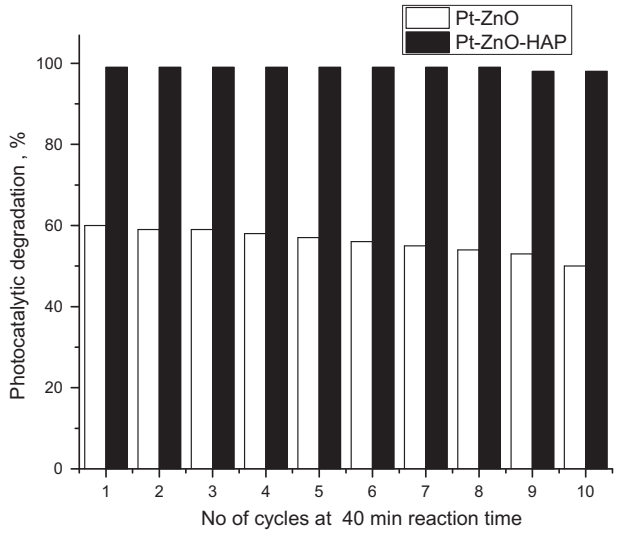

Fig. 10. Photochemical stability of Pt–ZnO and Pt–ZnO–HAP.

photodegradation of benzene were performed in Pt–ZnO and Pt–ZnO–HAP samples, and the results are shown in Fig. 10. After each photocatalytic reaction, the sample was left for reuse without further treatment. As shown in Fig. 8, 60% of benzene (40 min reaction time) could be degraded when Pt–ZnO sample is used for the first time. However, after 10 recycles, a significant decrease of photocatalytic activity for Pt–ZnO samples is found, and only 50% of benzene is degraded within 40 min. In contrast, the reused Pt–ZnO–HAP samples show less change in photocatalytic activity, 99% of benzene could be degraded when Pt–ZnO–HAP sample is used for the first time and after ten recycles, about 98% of benzene is degraded within 40 min.

In other words, HAP modification cannot only improve the photocatalytic performance but also the long-term stability of Pt-doped ZnO nanocrystals. This result is significant from the view point of practical application, as the enhanced photocatalytic activity and prevention of catalyst deactivation will lead to more cost-effective operation.

4. Conclusions

HAP modified Pt–ZnO nanoparticles show a noticeably improved photocatalytic activity than that of the Pt–ZnO, undoped ZnO, and P_{25} nanoparticles. After modification by HAP and Pt particles, the BET specific surface areas of the undoped ZnO nanoparticle greatly increases. Mean while, the amount of hydroxyls on the surface of the ZnO nanoparticle clearly increased. The Pt–ZnO–HAP samples show the highest visible-light-induced photocatalytic activity and photochemical stability than all the other catalysts; its degradation rate constant is 2.88 times that of Pt–ZnO and 13 times that of P_{25}, respectively. This research will give some new insights into the plan and synthesis of highly active photocatalytic nanomaterials.

References

[1] Q. Lan, L. Zhang, G. Li, R. Vermeulen, R.S. Weinberg, M. Dosemeci, S.M. Rappaport, M. Shen, B.P. Alter, Y. Wu, W. Kopp, S. Waidyanatha, C. Rabkin, W. Guo, S. Chanock, R.B. Hayes, M. Linet, S. Kim, S. Yin, N. Rothman, M.T. Smith, Hematotoxicity in workers exposed to low levels of benzene, Science 306 (2004) 1774–1776.

[2] R.M. Alberici, W.F. Jardim, Photocatalytic destruction of VOCs in the gas-phase using titanium dioxide, Appl. Catal. B: Environ. 14 (1997) 55–68.

[3] F.B. Li, X.Z. Li, C.H. Ao, S.C. Lee, M.F. Hou, Enhanced photocatalytic degradation of VOCs using Ln^{3+}–TiO_2 catalysts for indoor air purification, Chemosphere 59 (2005) 787–800.

[4] C.M. Schmidt, A.M. Buchbinder, E. Weitz, F.M. Geiger, Photochemistry of the indoor air pollutant acetone on degussa P_{25} TiO_2 studied by chemical ionization mass spectrometry, J. Phys. Chem. A 111 (2007) 13023–13031.

[5] R.C.W. Lam, M.K.H. Leung, D.Y.C. Leung, L.L.P. Vrijmoed, W.C. Yam, S.P. Ng, Visible-light-assisted photocatalytic degradation of gaseous formaldehyde by parallel-plate reactor coated with Cr ion-implanted TiO_2 thin film, Sol. Energ. Mat. Sol. C 91 (2007) 54–61.

[6] Y. Xu, C.H. Langford, Enhanced photoactivity of a titanium (IV) oxide supported on ZSM5 and zeolite A at low coverage, J. Phys. Chem. 99 (1995) 11501–11507.

[7] G.P. Lepore, L. Persaud, C.H. Langford, Supporting titanium dioxide photocatalysts on silica gel and hydrophobically modified silica gel, J. Photochem. Photobiol. A: Chem. 98 (1996) 103–111.

[8] H. Yoneyama, T. Torimoto, Titanium dioxide/adsorbent hybrid photocatalysts for photodestruction of organic substances of dilute concentrations, Catal. Today 58 (2000) 133–140.

[9] T. Ibusuki, K. Takeuchi, Removal of low concentration nitrogen oxides through photoassisted heterogeneous catalysis, J. Mol. Catal. A: Chem. 88 (1994) 93–102.

[10] T. Hisanaga, K. Tanaka, Photocatalytic degradation of benzene on zeolite-incorporated TiO_2 film, J. Hazard. Mater. B93 (2002) 331–337.

[11] J. Mo, Y. Zhang, Q. Xu, R. Yang, Effect of TiO_2/adsorbent hybrid photocatalysts for toluene decomposition in gas phase, J. Hazard. Mater. 168 (2009) 276–281.

[12] C. Ooka, H. Yoshida, K. Suzuki, T. Hattori, Effect of surface hydrophobicity of TiO_2-pillared clay on adsorption and photocatalysis of gaseous molecules in air, Appl. Catal. A: Gen. 260 (2004) 47–53.

[13] C. Ooka, H. Yoshida, K. Suzuki, T. Hattori, Adsorption and photocatalytic degradation of toluene vapor in air on highly hydrophobic TiO_2 pillared clay, Chem. Lett. 32 (2003) 896–897.

[14] N. Takeda, M. Ohtani, T. Torimoto, S. Kuwabata, H. Yoneyama, Evaluation of diffusibility of adsorbed propionaldehyde on titanium dioxide-loaded adsorbent photocatalyst films from its photodecomposition rate, J. Phys. Chem. B 101 (1997) 2644–2649.

[15] Y. Komazaki, H. Shimizu, S. Tanaka, A new measurement method for nitrogen oxides in the air using an annular diffusion scrubber coated with titanium dioxide, Atmos. Environ. 33 (1999) 4363–4371.

[16] M. Czerniczyniec, S. Farías, J. Magallanes, D. Cicerone, Arsenic(V) adsorption onto biogenic hydroxyapatite: Solution composition effects, Water, Air, Soil Pollut. 180 (2007) 75–82.
[17] Y. Feng, J.-L. Gonga, G.-M. Zenga, Q.-Y. Niua, H.-Y. Zhang, C.-G. Niua, J.-H. Denga, M. Yana, Adsorption of Cd (II) and Zn (II) from aqueous solutions using magnetic hydroxyapatite nanoparticles as adsorbents, Chem. Eng. J. 162 (2010) 487–494.
[18] T. Kawai, C. Ohtsuki, M. Kamitakahara, M. Tanihara, T. Miyazaki, Y. Sakaguchi, S. Konagaya, Removal of Formaldehyde by hydroxyapatite layer biomimetically deposited on polyamide film, Environ. Sci. Technol. 40 (2006) 4281–4285.
[19] H. Anmin, L. Tong, L. Ming, C. Chengkang, L. Huiqin, M. Dali, Preparation of nanocrystals hydroxyapatite/TiO_2 compound by hydrothermal treatment, Appl. Catal. B: Environ. 63 (2006) 41–44.
[20] H. Nishikawa, K. Omamiuda, Photocatalytic activity of hydroxyapatite for methyl mercaptane, J. Mol. Catal. A: Chem. 179 (2002) 193–200.
[21] H. Nishikawa, Surface changes and radical formation on hydroxyapatite by UV irradiation for inducing photocatalytic activation, J. Mol. Catal. A: Chem. 206 (2003) 331–338.
[22] H. Nishikawa, A high active type of hydroxyapatite for photocatalytic decomposition of dimethyl sulfide under UV irradiation, J. Mol. Catal. A: Chem. 207 (2004) 149–153.
[23] M. Pratar Reddy, A. Venugopal, M. Subrahmanyam, Hydroxyapatite photocatalytic degradation of calmagite (an azo dye) in aqueous suspension, Appl. Catal. B: Environ. 69 (2007) 164–170.
[24] K. Ozeki, J.M. Janurudin, H. Aoki, Y. Fukui, Photocatalytic hydroxyapatite/titanium dioxide multilayer thin film deposited onto glass using an rf magnetron sputtering technique, Appl. Surf. Sci. 253 (2007) 3397–3401.
[25] J. Nathanael, D. Mangalaraj, P.C. Chen, N. Ponpandian, Mechanical and photocatalytic properties of hydroxyapatite/titania nanocomposites prepared by combined high gravity and hydrothermal process, Compos. Sci. Technol. 70 (2010) 419–425.
[26] J.G. Yu, Q.J. Xiang, M.H. Zhou, Preparation, characterization and visible-light-driven photocatalytic activity of Fe-doped titania nanorods and first-principles study for electronic structures, Appl. Catal. B: Environ. 90 (2009) 595–602.
[27] Z. Liu, P. Fang, S. Wang, Y. Gao, F. Chen, F. Zheng, Y. Liu, Y. Dai, Photocatalytic oxidation of ethanol vapors under visible light on CdS–TiO_2 nanocatalyst, J. Mol. Catal. A: Chem. 363–364 (2012) 159–165.
[28] A. Bansal, S. Madhavi, T. Tan, T.M. Lim, Effect of silver on the photocatalytic degradation of humic acid, Catal. Today 131 (2008) 250–254.